Evidence that Nek1 does not phosphorylate Rad54-S572 during recovery from IR

Ishita Ghosh, Md Imtiaz Khalil, and Arrigo De Benedetti*

Department of Biochemistry and Molecular Biology, LSU Health Sciences Center, Shreveport, USA

*Corresponding author: arrigo.debenedetti@lsuhs.edu; Tel: 318-675-5668

ABSTRACT

A main focus of the work in our lab is on the activity of Tousled Like Kinase 1 (TLK1) in the area of DNA Damage and Repair. As one of its key interactor, TLK1 phosphorylates NIMA related kinase 1 (Nek1), and Nek1 was reported by Spies et al. to phosphorylate and regulate the activity of the key HRR protein Rad54[1], which suggested an intriguing signal transduction pathway: TLK1>Nek1>Rad54. In an effort to confirm such relations, we now report that we have not been able to reproduce key findings from that study. Specifically, we found that Nek1 does not phosphorylate RAD54-S572 as was reported. We generated Nek1-KO mouse NT1 cells[2] and Nek1-Knock-down in Hek293 (same cells as in Spies et al.), and the pRAD54-S572 signal does not change with our custom Ab, with or w/o IR. When we used an Ab from Lobrich's lab, it detected an immunoreactive band of wrong size for RAD54, which also did not change after IR even in synchronized G2 cells, contrary to their report. We also note that their P-assignment was based on guessing a weak consensus Nek1 sequence, and that site-directed mutagenesis of RAD54-S572 failed to yield biological effects in their in in vitro studies[1]. To conclusively establish that S572 is not a site of phosphorylation of Nek1, we carried out a IVK with purified Nek1 and RAD54 followed by MS analysis of the phosphatides, which revealed several but not S572. We also could not reproduce their copurification of Nek1-RAD54 by coIP, calling into question this interaction.

INTRODUCTION

Each day our cells face many exogenous and endogenous challenges that threat the genomic stability. The DNA double strand break is the most lethal form of damage. The major mechanism to maintain the fidelity of genetic code is Homologous recombination repair (HRR). The central enzyme of this pathway is Rad54.[3] Rad54 is a well conserved protein of the Rad52 group, a generally well conserved group in eukaryotes. Rad54 is a motor protein that translocates along dsDNA in an ATP hydrolysis dependent manner.[4] In mammals, the RAD54 gene plays its most important role during early developmental stages.[5] The primary function of homologous recombination in mitotic cells is to repair double-strand breaks (DSBs) that form as a result of replication fork collapse, from processing of spontaneous damage, and from exposure to DNA-damaging agents like topoisomerase poisons.[6] Ideally known as the swiss-army knife of homologous recombination repair, Rad54 functions in different stages of HRR. Rad54 interacts with Rad51 and promotes DNA strand -exchange, translocates along donor template, remodels donor chromatin, promotes Branch-migration of Holliday Junctions.[7-10] With such multi-faceted role in vivo, any post-translational modification of Rad54 may alter its activity. Therefore, it is critical to understand the regulation of this error-free mode of DNA repair in cells.

RESULTS

Given the possibility of a TLK1>Nek1>Rad54 axis and its importance for HRR, we wanted to probe the pattern of pRad54-S572 in cells with perturbed TLK1 activity. In an initial communication with Marcus Lobrich, he stated that they had finished the original antiserum published in the Mol Cell paper but that they would ship us a replacement that was not well-characterized. We tested that antiserum during a time-course of recovery from IR of HEK293 cells, either control or expressing a dominant Nek1 kinase-hypoactive mutant (HEK N5)[11], which was expected to show reduced pRad54-S572 signal (Fig.1); and it was immediately obvious that there were problems. The main immunoreactive band ran on the gel faster than its expected position of ~80kDa for Rad54 (Fig1). The signal was not very clean as there were several other (presumably less specific) prominent bands. Most importantly, the intensity of the pRad54 did not increase after recovery from IR, as it was reported. Given the impossibility of reproducing that part of the work with the Ab they provided, we commissioned our own custom-made pRad54-S572 antiserum from Thermofisher. After the 3d boost, an ELISA showed that

the serum had a high titer (>2X10^5 dilution) and an affinity >100-fold for the phosphopeptide compared to unphosphorylated, even before affinity purification. To establish the specificity of the Ab and its dependence on Nek1, we carried out a siRNA-mediated knockdown of Nek1 in Hek293 cells, similarly to their Fig. 3D experiment. Despite the successful knock-down of Nek1 (Fig.2), we did not observe any change in the signal with our pRad54-S572 antiserum, which detected a band at the correct position for Rad54 and overlapping the signal obtained with a commercial (santa-cruz sc-166370) pan-Rad54 antiserum. This clearly indicated that Nek1 is unlikely to be the kinase responsible for phosphorylation of S572. Considering the possibility that there might still be sufficient Nek1 in the KD-cells to phosphorylate S572, we took advantage of a mouse PCa cell line in which we clonally knocked-out Nek1 via CRISPR/CAS9 to rule out such possibility. Surprisingly, there was no immunoreactive band with pRad54-S572 antiserum in either control or the Nek1-KO clone – note that these cells do express Rad54L and Rad54B (RNAseq data communicated by Xiuping Yu). In contrast, there was a strong band in HEK293, equally in control and Nek1-siRNA-KD cells (Fig. 3). This result suggests that despite the high sequence conservation between mouse and human (Fig. 3B), the pRad54-S572 is not found in mouse, and one should wonder whether such proposed phosphorylation is at all important. To probe this question further, we set out to establish if their report of Rad54-S572 phosphorylation after IR, and particularly in late G2, could be reproduced. We thus, synchronized Hek293 cells following release from G1/S block with HU and irradiated them in early G2 (Fig.4), repeating their experimental conditions. Contrary to what they reported, we found no increase in pRad54-S572 in either asynchronous or cells enriched G2 (Fig.5), for which 8h was reported in their paper as the maximal level of phosphorylation[1].

In order find truly unbiased evidence for the proposed phosphorylation of S572 by Nek1, we carried out an *in vitro* kinase (IVK) and MS phosphopeptides analysis of recombinant (and functional) RAD54 phosphorylated by highly purified Nek1, as described in[12]. Note that a IVK reaction does not imply that RAD54 in a true in vivo substrate of Nek1, but this was done (Fig. 6A) merely to replicate the conditions used by Spies et al. (Fig 3B) in order to assign the putative phosphorylated residue. Note that the only possible interpretation of their Fig 3B is that S572 is the primary, if not the only, phosphor-target of Nek1, since virtually all P32 labeling from the IVK reaction is lost with the GFP-RAD54-S572/A mutant protein. In complete disagreement with their published Fig.3B and their assumed phosphorylation of S572 as the only Nek1 target site, there were several residues phosphorylated in vitro – but not S572 (Fig. 6B). A complete list of all modified the peptides is shown (Table 1), and multiple Ser, Thr, and Tyr were found – note that Nek1 is a dual specificity kinase[13]. Note also that our preparation of Nek1 was fully active, as indicated also by its autophosphorylation at Y315 (MS data not shown), which is diagnostic of its level of activity. In conclusion, their assignment of S572 as the only phosphorylation site by Nek1 cannot be reproduced when analyzed correctly by MS instead of relying on a putative consensus sequence; and their results of Fig.3B remains very difficult to explain.

Finally, we were not able to reproduce the reported interaction between Nek1 and Rad54 by coIP, although we cannot rule out that this could be due to a technical failure. Nonetheless, key findings of their paper could not be reproduced. These include a failure to attribute the phosphorylation of S572 to Nek1, its dependency on IR-induced damage, and in general the significance of such Rad54 modification for HRR.

Acknowledgements. We thank Xinngui Shen (ORCID Xinggui Shen http://orcid.org/0000-0002-4002-967) of the Mass Spectrometry Core at LSU Health-Shreveport supported by LSU Health Shreveport Foundation, Center for Cardiovascular Diseases and Sciences, and Feist-Weiller Cancer Center. This work was supported by a grant from the Feist Weiller Cancer Center from LSUHSC, Shreveport, and DoD grant PC160398.

Figure Legends

Figure 1. 2X 10^6 HEK293 cells were seeded 24hrs prior to treatment and then cells were treated with 10Gy of I.R and allowed to recover for indicated times (hrs). 40µg of untreated control (C) and samples were loaded in 8% SDS-PAGE gel and probed with aliquot of antibody sample from Lobrich lab. Tubulin probed as loading control.

Figure 2. 0.3X10^6 HEK293 cells seeded in 6 well plate 24hrs prior to siRNA treatment. Lipofectamine 3000 was used as transfection reagent with indicated amount of siNek1. 40ug of total samples loaded in 8% SDS-PAGE gel and probed with indicated antibodies (Nek1- sc 398813; Rad54- sc 166370; pRad54-Custom generated-Thermofisher; GAPDH- CST #2118)

Figure 3. A) 40µg of cell lysate from NEK1 WT (Cnt), K.O #6 clone (in NT1 cells) and siRNA treated HEK293 cells and control (Cnt) loaded in 8% SDS-PAGE gel and probed for Nek1 and pRad54 (custom generated) antibody. Actin band shown as loading control. B) Human Rad54 and mouse Rad54 protein sequence alignment shown for the conservation of the S572 site.

Figure 4. Cell cycle analysis of HEK293 cells synchronised (asynchronous -Asyn) at G1/S with Hydroxyurea treatment and released for indicated times (as shown in schematic).

Figure 5. Synchronised and aynchronised HEK293 cells were untreated or irradiated (5 Gy) at G2 and allowed to recover for indicated times. 40ug of cell lysate was loaded in 8% SDS-PAGE gel and probed with indicated antibodies. Ku-70 probed for loading control.

Figure 6. Determination of the RAD54 phosphopetides obtained by IVK with purified Nek1. A) Picture of the Coomassie stained gel confirming the purity of the proteins is shown. B) Phospho-peptide map of purified human Rad54 protein in IVK assay with purified Nek1.

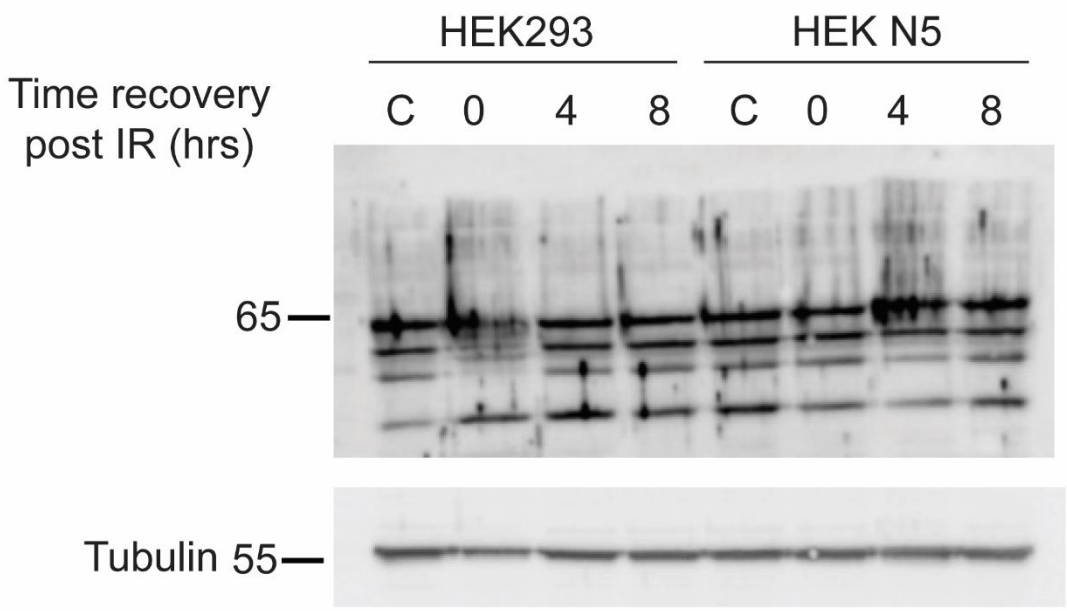
HEK293
HEK N5
Time recovery post IR (hrs)
C 0 4 8 C 0 4 8
65
Tubulin 55

Fig. 1

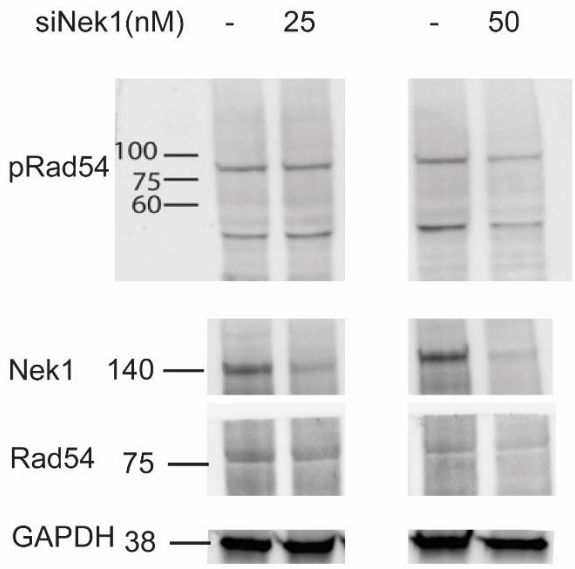
siNek1(nM) - 25 - 50
pRad54
100
75
60
Nek1 140
Rad54 75
GAPDH 38

Fig. 2

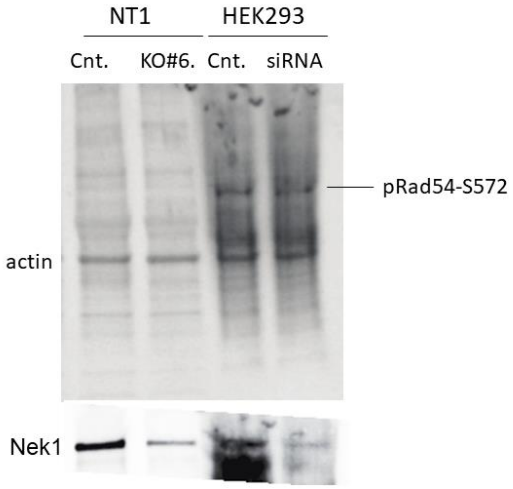

Fig.3A

```
hRad54 VRLDGTMSIKKRAKVVERFNSPSSPDFVFMLSSKAGGCGLNLIGANRLVMFDPDWNPAND 600
mRad54 VRLDGTMSIKKRAKVVERFNSPSSPDFVFMLSSKAGGCGLNLIGANRLVMFDPDWNPAND 600
```

Fig.3B

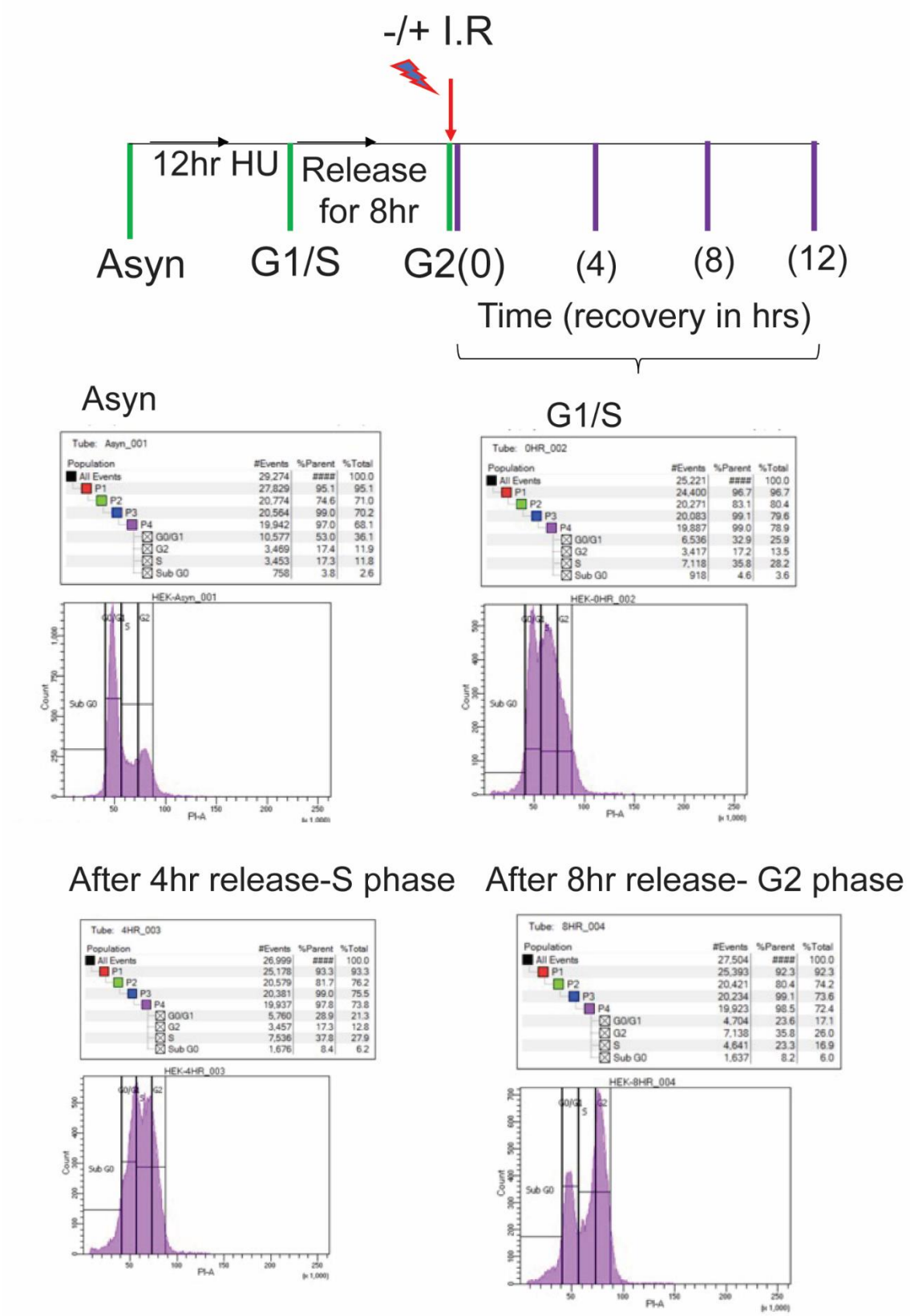
-/+ I.R
12hr HU
Release for 8hr
Asyn
G1/S
G2(0)
(4)
(8)
(12)
Time (recovery in hrs)
Asyn
Tube: Asyn_001
Population #Events %Parent %Total
All Events 29,274 #### 100.0
P1 27,829 95.1 95.1
P2 20,774 74.6 71.0
P3 20,564 99.0 70.2
P4 19,942 97.0 68.1
G0/G1 10,577 53.0 36.1
G2 3,469 17.4 11.9
S 3,453 17.3 11.8
Sub G0 758 3.8 2.6
HEK-Asyn_001
G0/G1
S
G2
Sub G0
Count
PI-A
G1/S
Tube: 0HR_002
Population #Events %Parent %Total
All Events 25,221 #### 100.0
P1 24,400 96.7 96.7
P2 20,271 83.1 80.4
P3 20,083 99.1 79.6
P4 19,887 99.0 78.9
G0/G1 6,536 32.9 25.9
G2 3,417 17.2 13.5
S 7,118 35.8 28.2
Sub G0 918 4.6 3.6
HEK-0HR_002
After 4hr release-S phase
Tube: 4HR_003
Population #Events %Parent %Total
All Events 26,999 #### 100.0
P1 25,178 93.3 93.3
P2 20,579 81.7 76.2
P3 20,381 99.0 75.5
P4 19,937 97.8 73.8
G0/G1 5,760 28.9 21.3
G2 3,457 17.3 12.8
S 7,536 37.8 27.9
Sub G0 1,676 8.4 6.2
HEK-4HR_003
After 8hr release- G2 phase
Tube: 8HR_004
Population #Events %Parent %Total
All Events 27,504 #### 100.0
P1 25,393 92.3 92.3
P2 20,421 80.4 74.2
P3 20,234 99.1 73.6
P4 19,923 98.5 72.4
G0/G1 4,704 23.6 17.1
G2 7,138 35.8 26.0
S 4,641 23.3 16.9
Sub G0 1,637 8.2 6.0
HEK-8HR_004

Fig.4

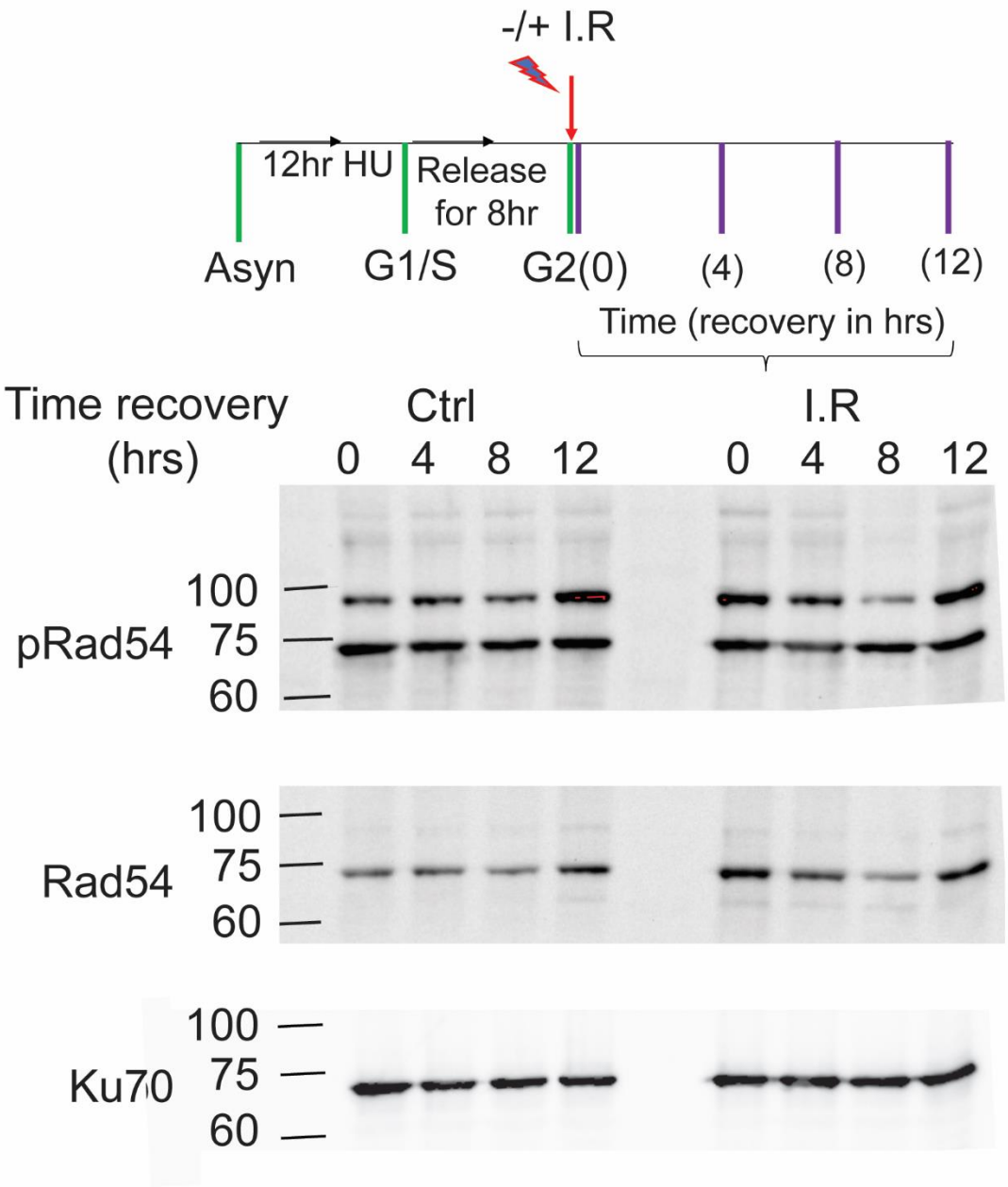
-/+ I.R
12hr HU
Release
for 8hr
Asyn
G1/S
G2(0)
(4)
(8)
(12)
Time (recovery in hrs)
Time recovery
(hrs)
Ctrl
I.R
0 4 8 12
0 4 8 12
100
75
60
pRad54
100
75
60
Rad54
100
75
60
Ku70

Fig. 5

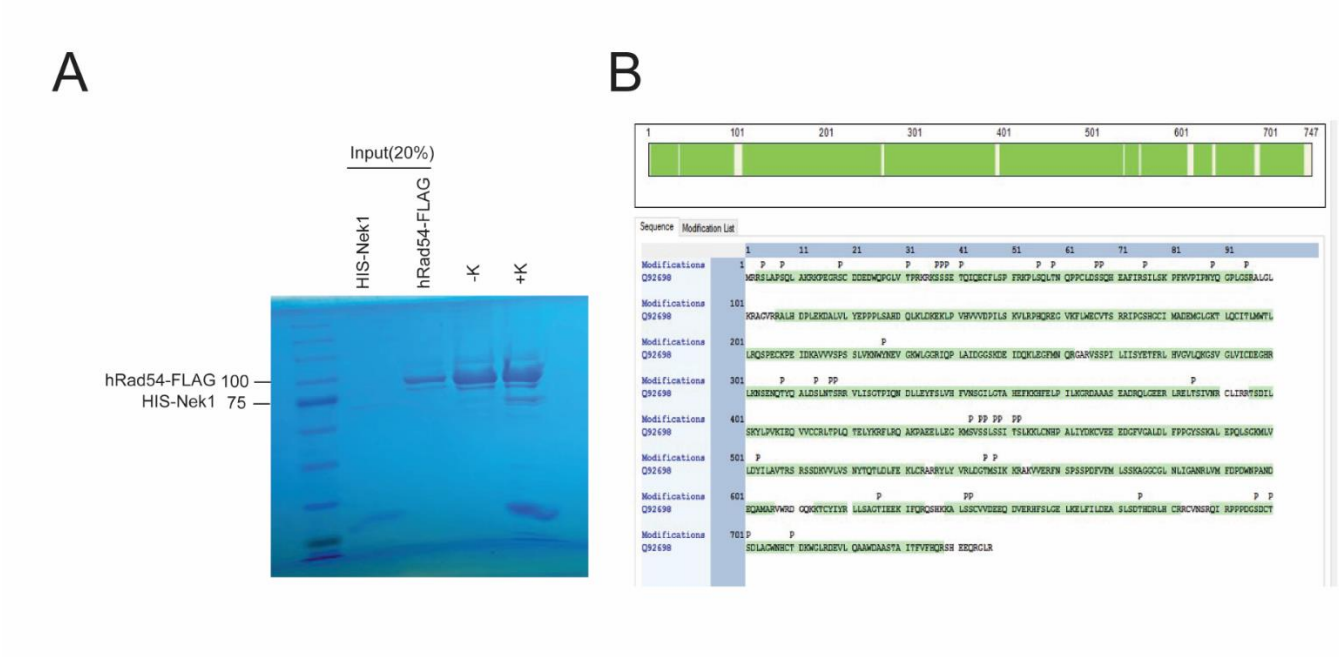

References

1 Spies, J. *et al.* Nek1 Regulates Rad54 to Orchestrate Homologous Recombination and Replication Fork Stability. *Mol Cell* **62**, 903-917, doi:10.1016/j.molcel.2016.04.032 (2016).

2 Khalil, M. I. *et al.* NEK1 Phosphorylation of YAP Promotes Its Stabilization and Transcriptional Output. *Cancers* **12**, 3666 (2020).

3 Symington, L. S. Role of RAD52 epistasis group genes in homologous recombination and double-strand break repair. *Microbiol Mol Biol Rev* **66**, 630-670, doi:10.1128/MMBR.66.4.630-670.2002 (2002).

4 Crickard, J. B., Moevus, C. J., Kwon, Y., Sung, P. & Greene, E. C. Rad54 Drives ATP Hydrolysis-Dependent DNA Sequence Alignment during Homologous Recombination. *Cell* **181**, 1380-1394.e1318, doi:https://doi.org/10.1016/j.cell.2020.04.056 (2020).

5 Essers, J. *et al.* Homologous and non-homologous recombination differentially affect DNA damage repair in mice. *EMBO J* **19**, 1703-1710, doi:10.1093/emboj/19.7.1703 (2000).

6 Mazin, A. V., Mazina, O. M., Bugreev, D. V. & Rossi, M. J. Rad54, the motor of homologous recombination. *DNA Repair (Amst)* **9**, 286-302, doi:10.1016/j.dnarep.2009.12.006 (2010).

7 Petukhova, G., Van Komen, S., Vergano, S., Klein, H. & Sung, P. Yeast Rad54 Promotes Rad51-dependent Homologous DNA Pairing via ATP Hydrolysis-driven Change in DNA Double Helix Conformation *. *Journal of Biological Chemistry* **274**, 29453-29462, doi:10.1074/jbc.274.41.29453 (1999).

8 Swagemakers, S. M. A., Essers, J., de Wit, J., Hoeijmakers, J. H. J. & Kanaar, R. The Human Rad54 Recombinational DNA Repair Protein Is a Double-stranded DNA-dependent ATPase *. *Journal of Biological Chemistry* **273**, 28292-28297, doi:10.1074/jbc.273.43.28292 (1998).

9 Zhang, Z., Fan, H.-Y., Goldman, J. A. & Kingston, R. E. Homology-driven chromatin remodeling by human RAD54. *Nature Structural & Molecular Biology* **14**, 397-405, doi:10.1038/nsmb1223 (2007).
10 Bugreev, D. V., Mazina, O. M. & Mazin, A. V. Rad54 protein promotes branch migration of Holliday junctions. *Nature* **442**, 590-593, doi:10.1038/nature04889 (2006).
11 Singh, V., Connelly, Z. M., Shen, X. & De Benedetti, A. Identification of the proteome complement of humanTLK1 reveals it binds and phosphorylates NEK1 regulating its activity. *Cell Cycle* **16**, 915-926 (2017).
12 Khalil, M. I. *et al.* NEK1 Phosphorylation of YAP Promotes Its Stabilization and Transcriptional Output. *Cancers (Basel)* **12**, doi:10.3390/cancers12123666 (2020).
13 Letwin, K. *et al.* A mammalian dual specificity protein kinase, Nek1, is related to the NIMA cell cycle regulator and highly expressed in meiotic germ cells. *Embo J* **11**, 3521-3531 (1992).

Confidenc	Sequence	Modificati	Qvality PEI	Qvality q-v	# Protein G	# Proteins	# PSMs	Master Prc	# Missed C
High	LVMFDPDV	2xOxidatio	3.95E-05	0.004739	1	1	79	Q92698	0
High	IEQVVCCR	2xCarbami	0.000465	0.004739	1	1	40	Q92698	0
High	TLQCITLMV	2xCarbami	0.103627	0.004739	1	1	1	Q92698	1
High	KLCNHPAL	2xCarbami	2.21E-07	0.004739	1	1	59	Q92698	2
High	LCNHPALIY	2xCarbami	4.37E-07	0.004739	1	1	97	Q92698	1
High	QIRPPPDG	2xCarbami	4.81E-06	0.004739	1	1	5	Q92698	0
High	QIRPPPDG	2xCarbami	9.26E-11	0.004739	1	1	38	Q92698	0
High	YLPVKIEQV	2xCarbami	0.0002	0.004739	1	1	58	Q92698	1
High	MLVLDYILA	1xPhospho	0.186682	0.004739	1	1	1	Q92698	0
High	NWYNEVG	1xPhospho	0.025781	0.004739	1	1	4	Q92698	0
High	LLSAGTIEE	1xPhospho	0.0006	0.004739	1	1	1	Q92698	0
High	LRELTSIVN	1xPhospho	0.128289	0.004739	1	1	1	Q92698	1
High	ELFILDEAS	1xPhospho	0.005986	0.004739	1	1	2	Q92698	0
High	SLAPSQLAI	1xPhospho	0.0191	0.004739	1	1	6	Q92698	0
High	RSLAPSQLA	1xPhospho	0.00741	0.004739	1	1	2	Q92698	1
High	SILSKPFK	1xPhospho	0.001382	0.004739	1	1	3	Q92698	0
High	VPIPNYQG	1xPhospho	0.025547	0.004739	1	1	4	Q92698	0
High	SILSKPFKV	1xPhospho	0.000224	0.004739	1	1	16	Q92698	1
High	LDGTMSIK	1xPhospho	0.010477	0.004739	1	1	3	Q92698	0
High	LKNSENQT	1xPhospho	0.003824	0.004739	1	1	9	Q92698	1
High	LKNSENQT	1xPhospho	0.011858	0.004739	1	1	8	Q92698	2
High	MSVSSLSSI	1xPhospho	0.003098	0.004739	1	1	12	Q92698	1
High	NSENQTYC	1xPhospho	0.000117	0.004739	1	1	5	Q92698	0
High	NSENQTYC	1xPhospho	0.000167	0.004739	1	1	16	Q92698	1
High	LVMFDPDV	1xOxidatio	2.01E-05	0.004739	1	1	90	Q92698	0
High	LDGTMSIK	1xOxidatio	0.001572	0.004739	1	1	39	Q92698	0
High	LDGTMSIK	1xOxidatio	0.00119	0.004739	1	1	15	Q92698	1
High	LEGFMNQI	1xOxidatio	0.003824	0.004739	1	1	27	Q92698	0
High	IQPLAIDGC	1xOxidatio	1.81E-06	0.004739	1	1	82	Q92698	2
High	MLVLDYILA	1xOxidatio	4.03E-06	0.004739	1	1	108	Q92698	0
High	MSVSSLSSI	1xOxidatio	4.98E-05	0.004739	1	1	22	Q92698	0
High	MSVSSLSSI	1xOxidatio	2.69E-06	0.004739	1	1	57	Q92698	1
High	FLRQAKPA	1xOxidatio	0.090318	0.004739	1	1	13	Q92698	2
High	FNSPSSPDI	1xOxidatio	0.000102	0.004739	1	1	52	Q92698	0
High	DEIDQKLEC	1xOxidatio	0.003576	0.004739	1	1	8	Q92698	1
High	ALEPQLSG	1xOxidatio	0.035362	0.004739	1	1	1	Q92698	1
High	EGVKFLWE	1xCarbami	0.000689	0.004739	1	1	3	Q92698	1
High	RIPGSHGC	1xCarbami	7.72E-07	0.004739	1	1	48	Q92698	1
High	RIPGSHGC	1xCarbami	2.86E-07	0.004739	1	1	69	Q92698	1
High	GSVGLVICI	1xCarbami	0.000188	0.004739	1	1	198	Q92698	0
High	GSVGLVICI	1xCarbami	0.00034	0.004739	1	1	1	Q92698	1
High	RIPGSHGC	1xCarbami	6.88E-08	0.004739	1	1	110	Q92698	1
High	IPGSHGCIN	1xCarbami	0.000937	0.004739	1	1	22	Q92698	0
High	IPGSHGCIN	1xCarbami	6.54E-06	0.004739	1	1	37	Q92698	0
High	IPGSHGCIN	1xCarbami	1.5E-08	0.004739	1	1	19	Q92698	0
High	KALSSCVVI	1xCarbami	1.58E-05	0.004739	1	1	14	Q92698	1

High	ALSSCVVD	1xCarbami	0.002291	0.004739	1	1	2	Q92698	0
High	ALSSCVVD	1xCarbami	7.16E-06	0.004739	1	1	25	Q92698	0
High	ALSSCVVD	1xCarbami	0.000106	0.004739	1	1	3	Q92698	1
High	FLWECVTS	1xCarbami	6.98E-05	0.004739	1	1	162	Q92698	0
High	FLWECVTS	1xCarbami	0.033493	0.004739	1	1	1	Q92698	1
High	QSPECKPE	1xCarbami	9.62E-05	0.004739	1	1	36	Q92698	0
High	QSPECKPE	1xCarbami	6.08E-05	0.004739	1	1	17	Q92698	1
High	TLQCITLM	1xCarbami	8.25E-05	0.004739	1	1	119	Q92698	0
High	AGGCGLNL	1xCarbami	2.13E-05	0.004739	1	1	22	Q92698	0
High	AGGCGLNL	1xCarbami	0.008985	0.004739	1	1	1	Q92698	1
High	TLQCITLM	1xCarbami	3.74E-06	0.004739	1	1	152	Q92698	0
High	KLCNHPAL	1xCarbami	8.56E-06	0.004739	1	1	68	Q92698	1
High	KTCYIYR	1xCarbami	0.000716	0.004739	1	1	9	Q92698	1
High	SCDDEDW	1xCarbami	0.01714	0.004739	1	1	6	Q92698	0
High	LCNHPALI	1xCarbami	4.64E-05	0.004739	1	1	131	Q92698	0
High	SCDDEDW	1xCarbami	2.62E-06	0.004739	1	1	20	Q92698	0
High	TCYIYR	1xCarbami	0.002952	0.004739	1	1	29	Q92698	0
High	FNSPSSPD	1xCarbami	0.00245	0.004739	1	1	2	Q92698	1
High	FNSPSSPD	1xCarbami	2.5E-06	0.004739	1	1	6	Q92698	1
High	CVEEEDGF	1xCarbami	3.49E-06	0.004739	1	1	154	Q92698	0
High	ELFILDEAS	1xCarbami	0.00092	0.004739	1	1	2	Q92698	1
High	ELFILDEAS	1xCarbami	0.000216	0.004739	1	1	11	Q92698	1
High	VVLVSNYT	1xCarbami	0.000245	0.004739	1	1	3	Q92698	1
High	MSVSSLSS	1xCarbami	6.57E-06	0.004739	1	1	1	Q92698	2
High	KPLSQLTN	1xCarbami	0.116337	0.004739	1	1	1	Q92698	0
High	KPLSQLTN	1xCarbami	5.2E-07	0.004739	1	1	27	Q92698	0
High	KPLSQLTN	1xCarbami	1.19E-09	0.004739	1	1	119	Q92698	0
High	KSSSETQIC	1xCarbami	0.000282	0.004739	1	1	11	Q92698	1
High	KSSSETQIC	1xCarbami	2.31E-06	0.004739	1	1	43	Q92698	1
High	SSSETQIQE	1xCarbami	5.36E-05	0.004739	1	1	24	Q92698	0
High	SSSETQIQE	1xCarbami	4.94E-06	0.004739	1	1	60	Q92698	0
High	ALEPQLSG		0.004906	0.004739	1	1	35	Q92698	0
High	ALEPQLSG		0.000164	0.004739	1	1	6	Q92698	1
High	ALEPQLSG		0.00071	0.004739	1	1	7	Q92698	2
High	ALHDPLEK		0.004028	0.004739	1	1	13	Q92698	0
High	ALHDPLEK		4.14E-08	0.004739	1	1	285	Q92698	1
High	ALHDPLEK		1.71E-09	0.004739	1	1	153	Q92698	2
High	AVVVSPSS		7.95E-05	0.004739	1	1	44	Q92698	0
High	AVVVSPSS		2.94E-05	0.004739	1	1	3	Q92698	1
High	DAAASEAD		0.001249	0.004739	1	1	1	Q92698	0
High	DAAASEAD		0.000106	0.004739	1	1	23	Q92698	1
High	DAAASEAD		0.026255	0.004739	1	1	1	Q92698	2
High	DALVLYEP		5.86E-05	0.004739	1	1	68	Q92698	0
High	DALVLYEP		1.32E-06	0.004739	1	1	27	Q92698	1
High	DALVLYEP		5.06E-07	0.004739	1	1	10	Q92698	2
High	DEIDQKLE		6.32E-05	0.004739	1	1	11	Q92698	1
High	DEVLQAAV		4.45E-07	0.004739	1	1	4	Q92698	0

High	DRPSVNSIL		0.00165	0.004739	1	1	1	Q96PY6	0
High	EKLPVHVV		5.14E-06	0.004739	1	1	72	Q92698	1
High	ELFILDEAS		1.5E-06	0.004739	1	1	222	Q92698	0
High	ELTSIVNR		0.001595	0.004739	1	1	10	Q92698	0
High	EVAVLANM		0.142523	0.004739	1	1	3	Q96PY6	0
High	FNSPSSPDI		2.17E-06	0.004739	1	1	133	Q92698	0
High	GRDAAASE		2.46E-06	0.004739	1	1	17	Q92698	2
High	HFELPILK		3.79E-05	0.004739	1	1	176	Q92698	0
High	HFELPILKG		0.004021	0.004739	1	1	4	Q92698	1
High	HFSLGELK		4.79E-05	0.004739	1	1	207	Q92698	0
High	HFSLGELKE		4.38E-08	0.004739	1	1	139	Q92698	1
High	HPNIVQYR		0.004413	0.004739	1	1	2	Q96PY6	0
High	KHFELPILK		0.001088	0.004739	1	1	120	Q92698	1
High	LDGTMSIK		0.000439	0.004739	1	1	37	Q92698	0
High	LDGTMSIK		0.002048	0.004739	1	1	9	Q92698	1
High	LDGTMSIK		0.038011	0.004739	1	1	1	Q92698	2
High	LDKEKLPVI		2.99E-08	0.004739	1	1	177	Q92698	2
High	LEGFMNQI		0.001825	0.004739	1	1	35	Q92698	0
High	IGEGSFGK		0.003307	0.004739	1	1	1	Q96PY6	0
High	LHVGVLQK		0.0009	0.004739	1	1	88	Q92698	0
High	LKNSENQT		7.35E-06	0.004739	1	1	36	Q92698	1
High	LKNSENQT		0.000206	0.004739	1	1	11	Q92698	2
High	LLSAGTIEE		0.000128	0.004739	1	1	151	Q92698	0
High	LLSAGTIEE		6.68E-05	0.004739	1	1	3	Q92698	1
High	LPVHVVVD		6.57E-06	0.004739	1	1	167	Q92698	0
High	LPVHVVVD		0.000305	0.004739	1	1	4	Q92698	1
High	IQPLAIDGG		0.001598	0.004739	1	1	8	Q92698	0
High	IQPLAIDGG		8.82E-06	0.004739	1	1	89	Q92698	1
High	IQPLAIDGG		1.11E-07	0.004739	1	1	165	Q92698	2
High	LRELTSIVN		0.000748	0.004739	1	1	183	Q92698	1
High	LTPLQTELY		0.000356	0.004739	1	1	40	Q92698	0
High	LTPLQTELY		2.78E-05	0.004739	1	1	94	Q92698	1
High	LTPLQTELY		0.219871	0.004739	1	1	1	Q92698	2
High	LVMFDPDV		5.77E-06	0.004739	1	1	114	Q92698	0
High	IVQNILGNE		0.024054	0.004739	1	1	2	Q96PY6	0
High	MLVLDYILA		5.63E-06	0.004739	1	1	98	Q92698	0
High	MSVSSLSSI		0.000209	0.004739	1	1	19	Q92698	0
High	MSVSSLSSI		7.73E-06	0.004739	1	1	119	Q92698	1
High	NSENQTYC		7.47E-07	0.004739	1	1	47	Q92698	0
High	NSENQTYC		0.000207	0.004739	1	1	13	Q92698	1
High	NWYNEVG		0.005236	0.004739	1	1	88	Q92698	0
High	NWYNEVG		0.000543	0.004739	1	1	5	Q92698	1
High	QAKPAEEL		5.04E-05	0.004739	1	1	119	Q92698	0
High	QAKPAEEL		0.00054	0.004739	1	1	1	Q92698	1
High	QAKPAEEL		0.001735	0.004739	1	1	2	Q92698	2
High	RALHDPLE		0.006919	0.004739	1	1	4	Q92698	1
High	RALHDPLE		9.54E-09	0.004739	1	1	236	Q92698	2

High	RSLAPSQLA		9.69E-05	0.004739	1	1	10	Q92698	1
High	RSLAPSQLA		0.121563	0.004739	1	1	1	Q92698	2
High	RVLISGTPI		0.001506	0.004739	1	1	32	Q92698	1
High	RYLYVR		0.005017	0.004739	1	1	82	Q92698	1
High	SLAPSQLAI		0.002679	0.004739	1	1	38	Q92698	0
High	SLAPSQLAI		0.013897	0.004739	1	1	3	Q92698	2
High	SILSKPFK		0.001511	0.004739	1	1	30	Q92698	0
High	SILSKPFKV		1.49E-07	0.004739	1	1	129	Q92698	1
High	SSDKVVLV		1.28E-06	0.004739	1	1	265	Q92698	1
High	TSDILSK		0.000624	0.004739	1	1	11	Q92698	0
High	TSDILSKYL		0.001429	0.004739	1	1	4	Q92698	1
High	VLISGTPIQ		9.12E-09	0.004739	1	1	38	Q92698	0
High	VLISGTPIQ		1.38E-08	0.004739	1	1	70	Q92698	1
High	VPIPNYQG		4.87E-05	0.004739	1	1	70	Q92698	0
High	VSSPILIISY		4.33E-06	0.004739	1	1	209	Q92698	0
High	VSSPILIISY		0.023489	0.004739	1	1	46	Q92698	1
High	VVERFNSP		0.028862	0.004739	1	1	1	Q92698	1
High	VVLVSNYT		4.09E-06	0.004739	1	1	179	Q92698	0
High	WGLRDEV		0.009857	0.004739	1	1	1	Q92698	1

Theo. MH+	Confidence	Percolator	Percolator	XCorr (by Search Engine): Sequest HT
2251.975	High	0.000146	1.1E-12	2.59
1063.502	High	0.000146	3.86E-10	2.22
2960.504	High	0.000146	0.000185	0.78
3868.856	High	0.000146	6.31E-16	4.02
3740.761	High	0.000146	6.31E-16	4.44
2807.155	High	0.000146	7.31E-15	6.22
2727.189	High	0.000146	6.31E-16	7.75
1663.866	High	0.000146	5.17E-11	2.79
1486.774	High	0.000146	0.000872	0.64
1089.44	High	0.000146	5.74E-06	1.33
1140.555	High	0.000146	7.07E-10	2.32
1280.672	High	0.000146	0.000322	1.97
1940.864	High	0.000146	1.7E-07	2.53
994.4969	High	0.000146	2.78E-06	1.89
1150.598	High	0.000146	2.83E-07	3.12
999.5275	High	0.000146	5.15E-09	1.93
1477.72	High	0.000146	5.61E-06	2.71
2378.263	High	0.000146	6.78E-11	4.92
944.4159	High	0.000146	6.5E-07	2.09
2262.04	High	0.000146	5.83E-08	3.36
2418.141	High	0.000146	8.77E-07	4.91
1547.775	High	0.000146	3.53E-08	2.31
2020.861	High	0.000146	1.45E-11	4.73
2176.962	High	0.000146	3.37E-11	5.02
2235.98	High	0.000146	2.2E-13	4.2
880.4445	High	0.000146	7.02E-09	1.84
1008.539	High	0.000146	3.62E-09	2.37
1010.472	High	0.000146	5.83E-08	2.12
2818.404	High	0.000146	7.81E-16	4.53
1422.803	High	0.000146	4.82E-15	2.59
1355.709	High	0.000146	1.9E-12	3.38
1483.804	High	0.000146	1.84E-15	4.28
3065.655	High	0.000146	0.00013	1.63
1805.841	High	0.000146	1.06E-11	3.26
1738.806	High	0.000146	4.96E-08	3.2
2346.31	High	0.000146	1.24E-05	0.87
1610.8	High	0.000146	9.81E-10	2.93
1960.904	High	0.000146	6.31E-16	5.95
1944.909	High	0.000146	6.31E-16	5.9
1398.679	High	0.000146	4.5E-11	3.78
1639.858	High	0.000146	1.83E-10	2.43
1928.914	High	0.000146	6.31E-16	5.66
1804.803	High	0.000146	2.05E-09	2.87
1788.808	High	0.000146	1.52E-14	3.88
1772.813	High	0.000146	6.31E-16	5.49
1863.875	High	0.000146	1.23E-13	5.14

1815.747	High	0.000146	1.72E-08	3.29
1735.78	High	0.000146	1.88E-14	3.73
2647.267	High	0.000146	1.15E-11	3.56
1197.572	High	0.000146	4.24E-12	1.96
1353.673	High	0.000146	1.09E-05	1.5
1330.631	High	0.000146	9.08E-12	2.86
2397.269	High	0.000146	3.04E-12	2.78
1664.886	High	0.000146	6.31E-12	2.56
1272.648	High	0.000146	2.52E-13	3.46
3473.615	High	0.000146	4.5E-07	1.76
1648.891	High	0.000146	4.04E-15	2.95
1471.773	High	0.000146	2.88E-14	4.49
1003.503	High	0.000146	1.08E-09	2.42
1854.736	High	0.000146	2.13E-06	3.13
1343.678	High	0.000146	1.61E-12	3.91
1774.77	High	0.000146	1.73E-15	4.38
875.408	High	0.000146	3.14E-08	1.09
3059.471	High	0.000146	2.02E-08	1.18
3043.476	High	0.000146	1.55E-15	3.72
2416.101	High	0.000146	3.4E-15	4.99
2507.138	High	0.000146	1.96E-09	4.92
2427.172	High	0.000146	6.2E-11	3.93
2298.216	High	0.000146	8.44E-11	3.95
2792.469	High	0.000146	1.53E-14	5.08
2826.268	High	0.000146	0.00025	1.22
2746.302	High	0.000146	6.31E-16	5.13
2666.336	High	0.000146	6.31E-16	7.06
2123.947	High	0.000146	1.17E-10	4.61
2043.98	High	0.000146	1.27E-15	5.02
1995.852	High	0.000146	2.26E-12	4.04
1915.885	High	0.000146	7.81E-15	3.28
942.5255	High	0.000146	1.06E-07	1.93
2330.315	High	0.000146	3.26E-11	2.8
2573.448	High	0.000146	1.05E-09	2.82
922.4993	High	0.000146	6.6E-08	2.47
2909.541	High	0.000146	6.31E-16	7.56
3265.747	High	0.000146	6.31E-16	7
1085.656	High	0.000146	5.78E-12	2.36
2076.112	High	0.000146	5.45E-13	4.28
905.3959	High	0.000146	4.05E-09	1.99
1617.746	High	0.000146	1.16E-11	3.81
1886.931	High	0.000146	6E-06	2.18
2006.059	High	0.000146	2.8E-12	3.17
2362.265	High	0.000146	6.31E-16	3.91
2619.403	High	0.000146	6.31E-16	5.69
1722.812	High	0.000146	3.35E-12	1.94
2476.226	High	0.000146	6.31E-16	5.07

1257.68	High	0.000146	7.87E-09	2.52
1673	High	0.000146	8.58E-15	3.32
1860.897	High	0.000146	6.31E-16	4.19
931.5207	High	0.000146	7.25E-09	1.99
974.5339	High	0.000146	0.000425	1.23
1789.847	High	0.000146	1.1E-15	2.37
1830.869	High	0.000146	1.49E-15	3.79
996.5877	High	0.000146	9.92E-13	2.6
1209.71	High	0.000146	6.58E-08	2.99
930.5043	High	0.000146	1.74E-12	2.6
2772.384	High	0.000146	6.31E-16	5.33
1026.548	High	0.000146	8.22E-08	1.74
1124.683	High	0.000146	2.92E-09	2.18
864.4495	High	0.000146	3.37E-10	2.05
992.5445	High	0.000146	1.32E-08	1.66
1148.646	High	0.000146	1.49E-05	1.31
2029.206	High	0.000146	6.31E-16	7.2
994.4775	High	0.000146	9.99E-09	2.04
794.4043	High	0.000146	4.12E-08	1.3
893.5567	High	0.000146	1.86E-09	2.08
2182.073	High	0.000146	2.01E-14	5.76
2338.175	High	0.000146	5.57E-11	4.39
1060.588	High	0.000146	1.79E-11	1.45
1604.901	High	0.000146	3.82E-12	3.8
1415.862	High	0.000146	1.54E-14	4.2
2302.387	High	0.000146	1.41E-10	2.19
1098.615	High	0.000146	7.29E-09	2.17
1826.949	High	0.000146	3.09E-14	3.5
2802.409	High	0.000146	6.31E-16	5.64
1200.706	High	0.000146	1.19E-09	3.32
1205.678	High	0.000146	2.05E-10	1.75
1361.779	High	0.000146	4.74E-13	3.24
1778.032	High	0.000146	0.001359	1.3
2219.985	High	0.000146	1.13E-14	3.4
1877.003	High	0.000146	4.86E-06	1.35
1406.808	High	0.000146	1.07E-14	2.84
1339.714	High	0.000146	5.74E-11	2.95
1467.809	High	0.000146	2.26E-14	4.31
1940.894	High	0.000146	6.31E-16	3.55
2096.996	High	0.000146	5.61E-11	4.6
1009.474	High	0.000146	1.24E-07	1.75
1578.781	High	0.000146	5.6E-10	2.26
1312.711	High	0.000146	1.96E-12	3.42
2633.407	High	0.000146	5.51E-10	3.62
2761.502	High	0.000146	8.85E-09	3.66
1078.6	High	0.000146	2.41E-07	2.31
3065.642	High	0.000146	6.31E-16	5.9

1070.632	High	0.000146	9.28E-12	2.74
1226.733	High	0.000146	0.000281	1.13
3915.08	High	0.000146	6.32E-09	1.88
869.4992	High	0.000146	1.12E-07	1.39
914.5306	High	0.000146	2.5E-08	1.7
1637.945	High	0.000146	1.28E-06	2.07
919.5611	High	0.000146	6.38E-09	2.21
2298.297	High	0.000146	6.31E-16	4.59
2286.186	High	0.000146	6.31E-16	3.75
763.4196	High	0.000146	7.78E-10	1.89
1363.783	High	0.000146	5.6E-09	3.34
3758.979	High	0.000146	6.31E-16	7.77
3887.074	High	0.000146	6.31E-16	7.48
1397.754	High	0.000146	1.8E-12	2.17
1624.894	High	0.000146	5.7E-15	2.46
2499.433	High	0.000146	4.57E-06	0.98
2273.127	High	0.000146	7.56E-06	3.16
1869	High	0.000146	4.99E-15	4.39
2988.512	High	0.000146	5.62E-07	1.46